Evolution of gold nanoparticles through Catalan, Archimedean, and Platonic solids†

Do Youb Kim,‡[a] Sang Hyuk Im,‡*[b] O. Ok Park*[a] and Yong Taik Lim[c]

Received 16th July 2009, Accepted 11th September 2009
First published as an Advance Article on the web 22nd September 2009
DOI: 10.1039/b914353j

This paper reports the transformation of rhombic dodecahedral gold nanoparticles through two different pathways depending on the water content. The gold nanoparticles were prepared by reducing $HAuCl_4$ with *N,N*-dimethylforamide in the presence of poly(vinyl pyrrolidone) and water. Not only the concentration of PVP but also the water content has a critical role in determining the shape transformation of the gold nanocrystals. At low water content the rhombic dodecahedron is transformed into a rhombicuboctahedron to a truncated octahedron and then to an octahedron, while at higher water content the rhombic dodecahedron is transformed into a rhombicuboctahedron and then to a cube or a truncated cube and then to a cuboctahedron and to a truncated octahedron. In addition, we demonstrated cell imaging by using the truncated octahedral, rhombic dodecahedral and octahedral gold nanoparticles as a contrast agent.

Introduction

The control of the shape and morphology of metal nanocrystals has been intensively studied in recent years in order to investigate the strong correlation between their shapes and their optical, electronic, chemical, physical, and catalytic properties.[1–6] In particular, gold nanocrystals have attracted considerable attention because of their numerous applications, such as in surface plasmonics, surface-enhanced Raman scattering (SERS), photothermal therapy, as well as in chemical and biological sensing.[7–11] Various synthetic methods based on colloidal chemistry have already provided routes for the production of shape-controlled gold nanoparticles such as Platonic solids,[12–14] decahedra,[15] rods,[16] plates,[3] and multipods.[17] The seed-mediated growth of gold nanoparticles has recently been used to demonstrate transformations between nanoparticles with various shapes such as rod to octahedron[18] and cube to cuboctahedron to octahedron;[19] this latter transformation shows the possibilities for nanocrystals with octahedral symmetry (O_h). However, rhombic dodecahedral nanoparticles composed of twelve {110} facets have been difficult to achieve even though they have the same O_h symmetry as cubes and octahedra, because the surfaces of gold nanocrystals tend to exhibit facets in the order {111} > {100} > {110} among the lowest index planes to minimize their surface energies.[20,21] Here we report that a rhombic dodecahedron can be directly transformed to an octahedron through two different pathways depending on the water content. At low water content, the rhombic dodecahedron is transformed into a rhombicuboctahedron to a truncated octahedron and then to an octahedron, while at higher water content, the rhombic dodecahedron is transformed into a rhombicuboctahedron and then to a cube or a truncated cube and then to a cuboctahedron and to a truncated octahedron. In addition, we demonstrated cell imaging by using the truncated octahedral, rhombic dodecahedral and octahedral gold nanoparticles.

Experimental

Materials

N,N-Dimethylformamide (DMF: Sigma-Aldrich), hydrogen tetrachloroaurate trihydrate ($HAuCl_4 \cdot 3H_2O$: Sigma-Aldrich), and poly(vinylpyrrolidone) (PVP: Aldrich, Mw = 55 000) were obtained from Sigma-Aldrich and used without further purification. High-purity deionized water (18.3 MΩ cm^{-1}) was produced using Pure Power water purification system (Human, Korea).

Synthesis of gold nanoparticles

In a typical synthesis, 3.5 mL DMF and 1.4 mL water are added to 0.1 mL of 94.2 mM $HAuCl_4$ with 7 mL of 1.46 mM PVP in DMF; this solution is placed in a 50 mL vial, which is then capped and heated with stirring in an oil bath at 120 °C for 2 h. To observe the size and shape change of the particles during the reaction, the reactants were picked out and quenched by ice bath at certain times. The final solution was cooled, and the particles were collected by centrifugation at 13 000 rpm and purified by dispersion/precipitation cycle with water and ethanol to remove excess PVP. The product was finally dispersed in ethanol for

[a]*Department of Chemical and Biomolecular Engineering (BK21), Korea Advanced Institute of Science and Technology (KAIST), 335 Gwahangno, Yuseong-gu, Daejeon, 305-701, Korea. E-mail: ookpark@kaist.ac.kr; Fax: +82-42-350-3910; Tel: +82-42-350-3923*
[b]*KRICT-RPFL Global Research Laboratory, Advanced Materials Division, Korea Research Institute of Chemical Technology, 19 Singsungno, Yuseong-gu, Daejeon, 305-600, Korea. E-mail: imromy@krict.re.kr*
[c]*Korea Research Institute of Bioscience and Biotechnology (KRIBB), 111 Gwahangno, Yuseong-gu, Daejeon, 305-806, Korea*
† Electronic supplementary information (ESI) available: Materials, detailed descriptions of experimental procedures, three additional figures and analyses. See DOI: 10.1039/b914353j
‡ These authors equally contributed to this work.

SEM and TEM characterization or DPBS (Dulbecco's Phosphate Buffered Saline, 1×, Gibco) for cell imaging.

Characterization

SEM images were recorded with a field-emission scanning electron microscope (Sirion, FEI) operating at an accelerating voltage of 10∼20 kV. TEM images and SAED patterns were obtained using a field-emission transmission electron microscope (JEM-2100F, JEOL) operating at an accelerating voltage of 200 kV. The samples were prepared by putting a few drops of colloidal solutions either on silicon wafer for SEM or on copper grids coated with carbon film for TEM and SAED. The UV-Vis absorption data were collected on a UV-Vis spectrophotometer (Cary 100, Varian) using colloidal ethanol suspension.

Cell imaging

RAW264.7, a mouse macrophage cell line, was obtained from the ATCC (Manassas, VA). Cells were cultured in Dulbecco's Modified Eagle's Medium (DMEM, Gibco, USA) supplemented with 2 mM glutamine, antibiotics (100 μg mL-1 penicillin and 50 μg/mL streptomycin), and 10% (v/v) fetal bovine serum (FBS, Gibco, USA) at 37 °C under 5% (v/v) CO_2. RAW264.7 cells (5×10^5/mL) were also prepared in 24-well plates. 500 μL of DPBS was used to wash cells before experiments. PEG-coated gold NPs (truncated octahedral (540 nm), rhombic dodecahedral (565 nm), octahedral (603 nm), the optical density at each plasmon resonance wavelength was matched to 1.0) (350 μL) were then added to the RAW264.7 cells and the mixture was incubated at 37 °C for 1 h. After washing with 500 μL DPBS three times to remove unattached gold NPs, 300 μL of McCoy's 5A medium containing 10 % [v/v] FBS and antibiotics were added. Light-scattering images of RAW264.7 cells treated with gold NPs were obtained using an inverted dark-field microscope (Nikon). A narrow beam of light from a tungsten source was delivered with a dark-field condenser, and only scattered light from samples was collected, using a 100×/1.35 oil Iris objective (Uplanapo).

Results and discussion

In the colloidal chemistry of gold nanoparticles, N,N-dimethylformamide (DMF) is often used as both a solvent and a reducing agent for the gold salt. Gold atoms can be obtained by reducing $HAuCl_4$ with DMF in the presence of water *via* the following reaction:[22]

$$2HAuCl_4 + 3HCON(CH_3)_2 + 3H_2O \leftrightarrow 2Au + 3(CH_3)_2NCOOH + 8H^+ + 8Cl^- \quad (1)$$

Once the concentration of gold atoms reaches the supersaturation value after the dissociation and reduction of the gold salt, gold nuclei are generated and nanoparticles form. During the growth of the nanocrystals, the addition of poly(vinylpyrrolidone) as a capping agent can be used to regulate the shape of the resulting particles by stabilizing certain facets of the nanoparticles and preventing the aggregation of gold on other facets. PVP has a critical role in determining the shape of the nanocrystals, but the water concentration is also expected to affect this process (see Fig. S1, 2, ESI†). Water enables the gold salts to dissociate into gold ions, which are readily reduced to gold atoms by DMF, but it also accelerates the forward reaction. At the same time, it promotes the generation of protons and chloride ions, which can dissolve or etch twinned particles or sharpened edges through the backward oxidative etching reaction.[23]

Firstly for a model system about low water content, we examined the growth of the gold particles resulting from the addition of 1.4 mL of water as a function of the reaction time.

Note that we can only get the octahedral gold nanoparticles in high yield at this water content when examining the shape of the produced particles according to the variation of the water content. In a typical synthesis, 3.5 mL DMF and 1.4 mL water are added to 0.1 mL of 94.2 mM $HAuCl_4$ with 7 mL of 1.46 mM PVP in DMF; this solution is placed in a 50 mL vial, which is then capped and heated with stirring in an oil bath at 120 °C for 2 h. The primary stages of the reaction can be recognized by observation of their distinctive colors. In the initial stage, the color of the solution is light-yellow after all the chemicals (DMF, PVP, $HAuCl_4$, and H_2O) have been mixed, and gradually fades as the solution becomes transparent and colorless within ∼3 min; this color change corresponds to the conversion of Au(III) into Au(I).[14] The solution turns reddish in color in around ∼4 min, which indicates that Au(I) has been reduced to Au(0) and that the supersaturated gold atoms have nucleated and nanoparticles have formed. Fig. 1a shows a TEM image of the resulting nanoparticles around ∼4 min, which shows that most of the particles are composed of small multiply twinned particles with a diameter of ∼20 nm, with some single particles with a diameter of ∼50 nm also present. This bimodal distribution is due to the selective etching and growth of the initially formed nanoparticles; the multiply twinned particles tend to disappear as a result of the etching of the highly reactive twinned boundaries, whereas the single nanocrystals survive and grow into larger ones. Fig. 1b shows an SEM image of the gold nanocrystals obtained in around 5 min 14 s, which shows the formation of the monodisperse rhombic dodecahedral single crystals (Catalan solids) with an edge length of ∼40 nm. The rhombic dodecahedral particles also exhibit sharp edges, which imply that the growth reaction dominates etching because the single crystals grow immediately at the expense of the twinned crystals during this stage. Surprisingly, it also clearly shows that the rhombic dodecahedral crystals formed initially can be transformed into octahedral nanocrystals in the end. The formation of rhombic dodecahedral nanoparticles during the initial stages is very unusual because generally for face centered cubic (fcc) structured metal nanocrystals smaller than 10∼20 nm, the surface tends to be polyhedral, *e.g.* cuboctahedral, and to form twinned seeds to minimize the surface energy. Fig. 1c shows the corresponding TEM image of the rhombic dodecahedral nanoparticles, which confirms the formation of single crystals with sharp edges. The right top inset shows a schematic illustration of a rhombic dodecahedron with its {110} facet parallel to the substrate; the electron diffraction pattern in the right hand bottom inset confirms the presence of the (110) plane. The rhombic dodecahedral nanoparticles are truncated at the edges around ∼6 min 30 s, as shown in Fig. 1d. The average diameter of the resulting particles is up to ∼85 nm, but the sharp edges of the {100} and {111} facets have been truncated because the etching reaction hinders the addition of gold atoms onto the sharp edges and

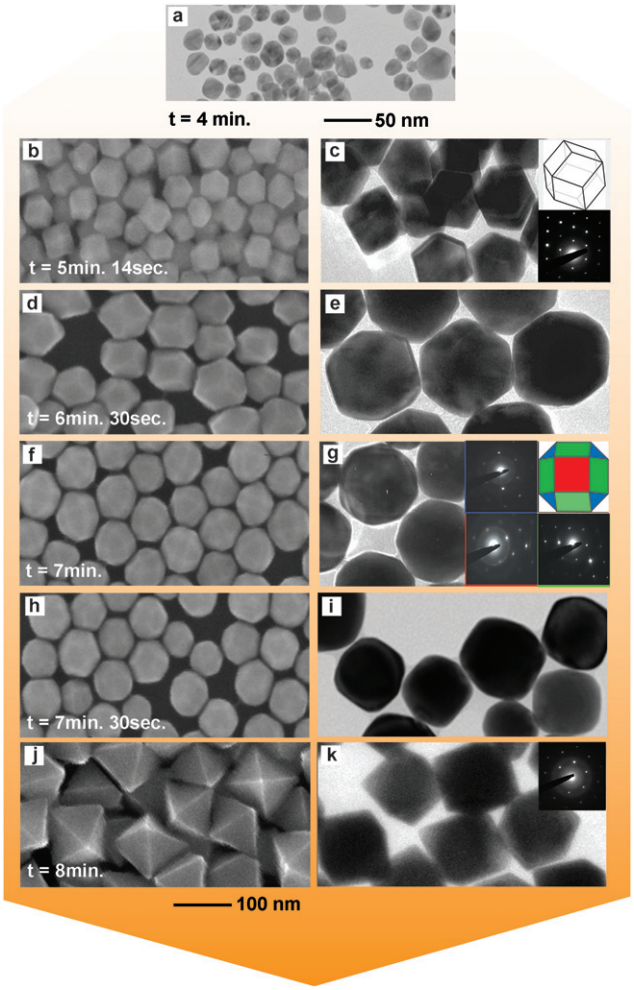

Fig. 1 SEM and TEM images showing the variation of the shape of gold nanocrystals in the presence of 1.4 mL of added water with the reaction time (t): (a) t = 4 min, (b),(c) t = 5 min 14 s, (d),(e) t = 6 min 30 s, (f),(g) t = 7 min, (h),(i) t = 7 min 30 s, (j),(k) t = 8 min (a), (c), (e), (g), (i), and (k) are TEM images. The scale bar is 50 nm. (c) The right top inset shows a schematic diagram of a rhombic dodecahedron with its {110} face parallel to the substrate and the right bottom inset shows its electron diffraction pattern. (g) The right top inset shows a schematic diagram of a rhombicuboctahedron with its {100} facet parallel to the substrate. The red, green, and blue colors correspond to the {100}, {110}, and {111} faces, respectively. The colors of the frames of the other insets showing the electron diffraction patterns of each face match the displayed color of the face. (k) The inset shows the electron diffraction pattern that confirms the presence of the {111} facet. (b), (d), (f), (h), and (j) are SEM images.

results in the promotion of selective growth in the <110> direction. Of course, at this stage it is still unclear that this shape transformation (truncation) is derived from either selective capping of certain facets by PVP or from selective etching of certain facets by a backward reaction since both routes can yield such shape transformation. Besides the effect of PVP, if explaining the results from the point of view of the etching reaction, the growth of particles in all dimensions seems to arise because growth still dominates etching, although etching hinders the growth in the <100> and <111> directions. Thus etching only reduces the growth rate in the <100> and <111> directions and enables anisotropic growth during this stage. The TEM image of these particles shown in Fig. 1e clearly confirms the formation of truncated rhombic dodecahedral single crystals. The truncated rhombic dodecahedral nanoparticles have been transformed into rhombicuboctahedral nanocrystals (Archimedean solids) in ~7 min by further truncation, as shown in Fig. 1f. The image of the rhombicuboctahedral nanoparticles clearly shows that the edges of the {100} and {111} facets have been cut by both the selective etching and the growth to form thermodynamically stable crystals. The crystals generally tend to grow in a direction that preferentially eliminates firstly the most unstable {110} facet and then the {100} facet and increases the fraction of the {111} facet. In addition, the size of the nanoparticles slightly decreases to ~80 nm in diameter as the shape of the nanocrystals is transformed by further truncation. This is a decisive evidence that the shape transformation during this intermediate stage is due not to selective capping but to selective etching because the shape evolution due to selective capping of certain facets should be accompanied by the enlargement of the nanocrystals due to the addition of metal atoms onto uncapped sites. The rhombicuboctahedral particles in the corresponding TEM image in Fig. 1g appear as octagons because the {100} faces of the particles are parallel to the substrate. The right top inset shows a schematic illustration of such a rhombicuboctahedron bound on the {100} (red), {110} (green), and {111} (blue) faces. To confirm the crystal structures of the particles we examined the SAED (selective area electron diffraction) pattern of each facet. The insets (the color of each frame matches the color of each facet) confirms again the formation of rhombicuboctahedra with {110}, {100}, and {111} facets. The rhombicuboctahedral particles have been transformed into truncated octahedral nanocrystals in ~7 min 30 s by further reactions, as shown in Fig. 1h. The diameter of the nanoparticles also slightly decreases to ~75 nm as a result of etching and growth. The truncated octahedral particles are bound only by {111} and {100} facets, which indicates that the etching reaction contributes mainly to the elimination of the edges and/or the hindrance of the addition of atoms onto the edges, and that the growth reaction proceeds toward surface energy minimization. Etching and growth transform the rhombicuboctahedron into a truncated octahedron as a result of the preferential elimination of the {110} facet. Fig. 1i shows a TEM image confirming the formation of truncated octahedral single crystals with slightly smaller dimensions than the rhombicuboctahedral particles. The truncated octahedral crystals have been transformed into octahedral particles (Platonic solids) with an edge length of ~75 nm at ~8 min as shown in Fig. 1j. The thermodynamically unstable {100} facet in the cuboctahedral particles is eliminated by further growth in the <100> direction and finally octahedral particles bound on the {111} face with sharp edges are formed. Thus the octahedral nanoparticles are transformed from rhombic dodecahedral crystals into a thermodynamically stable shape by etching and growth. The TEM image in Fig. 1k indicates the formation of octahedral single crystals with sharp edges and the inset confirms that the crystal structure is bound on the {111} face. The octahedral nanocrystals grow to become larger particles with an edge length of ~100 nm without truncation or shape transformation through further reaction.

Secondly for a model system with high water content, we examined again the growth of the gold particles resulting from

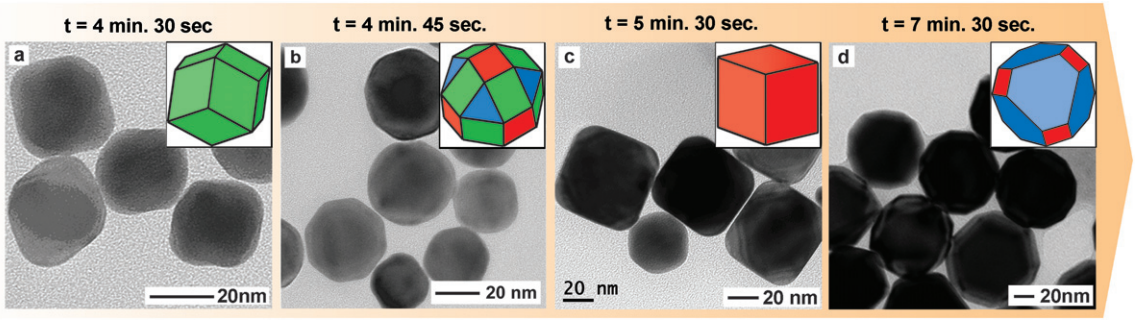

Fig. 2 TEM images of the gold nanoparticles resulting from the addition of 2 mL of water for various reaction times (t): (a) t = 4 min 30 s, (b) t = 4 min 45 s, (c) t = 5 min 30 s, and (d) 7 min 30 s. The insets show schematic illustrations of the resulting particles.

the addition of 2 mL of water as a function of the reaction time. Except for using 2.9 mL DMF and 2 mL of water, the other conditions were held constant. The evolution of the particle shapes during the early stages was characterized with TEM, as shown in Fig. 2. Fig. 2a shows a TEM image of the nanoparticles near ~4 min 30 s, which indicates that the truncated octahedral particles grow from rhombic dodecahedral seed particles with a diameter of ~30 nm as in the case of the octahedral crystals. The rhombic dodecahedral seeds are quickly transformed into rhombicuboctahedral nanocrystals with a diameter of ~35 nm by around ~4 min 45 s, as shown in Fig. 2b. Interestingly, the rhombicuboctahedral nanoparticles are then transformed into cubes or truncated cubes with a diameter of ~60 nm by around ~5 min 30 s, as shown in Fig. 2c. The cubic particles might form as a result of the suppression of addition onto the {100} face and the activation of addition onto the {110} and {111} faces due to the enhanced etching and growth. Although the shape transformation is mainly generated by etching in the case of the octahedral nanocrystals, the cubic shapes are generated by the growth reaction rather than by the etching reaction because the sizes of the resulting nanoparticles monotonically increase with reaction time. Although the preferential elimination of the {110} face arises due to the enhanced etching and growth (mainly consisting of the addition of gold atoms onto the {110} face), most of the rhombicuboctahedral nanoparticles are transformed into truncated cubes. The cubes or truncated cubes are then transformed into truncated octahedral nanoparticles with a diameter of ~80 nm by ~7 min 30 s *via* cuboctahedral nanocrystals by further growth, as shown in Fig. 2d. More etching as a result of the addition of more water can produce truncated octahedral nanocrystals, because the sharp edges do not survive under these conditions.

The schematic illustration in Fig. 3 summarizes the interparticle transformations between the rhombic dodecahedron bound on the {110} facet, the cube bound on the {100} facet, and the octahedron bound on the {111} facet. In these experimental conditions, the rhombic dodecahedral particles are formed initially and transformed to the truncated rhombic dodecahedra and then to the rhombicuboctahedra by etching and growth. The shape of rhombicuboctahedral nanoparticles are then transformed through two different pathways with water content. The addition of 1.4 mL of water transforms the octahedron into the rhombicuboctahedron *via* the truncated octahedron through the upper pathway. On the addition of 2 mL of water, the rhombicuboctahedron is transformed to a cube or a truncated cube to a cuboctahedron and then to a truncated octahedron through the lower pathway.

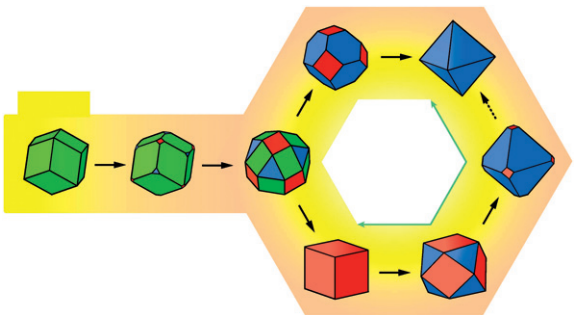

Fig. 3 A schematic diagram for the shape transformation of the gold nanocrystals with the water content. The addition of 1.4 mL of water transforms the octahedron into the rhombic dodecahedron *via* the rhombicuboctahedron and truncated octahedron through the upper pathway, which arises for slower growth. On the addition of 2 mL water, the rhombic dodecahedron is transformed *via* the rhombicuboctahedron to a cube or a truncated cube to a cuboctahedron and then to a truncated octahedron through the lower pathway, due to the strengthened etching and growth. The green line shows the transformation of a cube to an octahedron *via* the cuboctahedron and *vice versa*, as previously reported in the literature.[19]

It is very useful to characterize the optical properties of gold nanocrystals because of the sensitivity of these properties to both shape and size. UV/Vis absorption spectra were obtained during the transformation from the rhombic dodecahedron to the octahedron, which confirms the presence of the particles shown for each step in Fig. 4. The rhombic dodecahedral nanocrystals with an edge length of ~40 nm (~50 nm in diameter) exhibit a strong absorption peak at 565 nm, whereas the larger truncated rhombic dodecahedral particles with a diameter of ~85 nm absorb light at 550 nm because the surface charges accumulated at the sharp edges reduce the restoring force for electron oscillation and result in a red shift in the resonance peak; this result implies that the absorption peaks are more strongly dependent on the crystals' shapes than on their sizes.[24,25] The absorption peaks of the rhombicuboctahedral nanocrystals with a diameter of ~80 nm and the truncated octahedral particles with a diameter of ~75 nm are blue-shifted to 545 and 540 nm, respectively, by the additional rounding and contraction in dimensions. The absorption peak of the octahedral nanocrystals with an edge

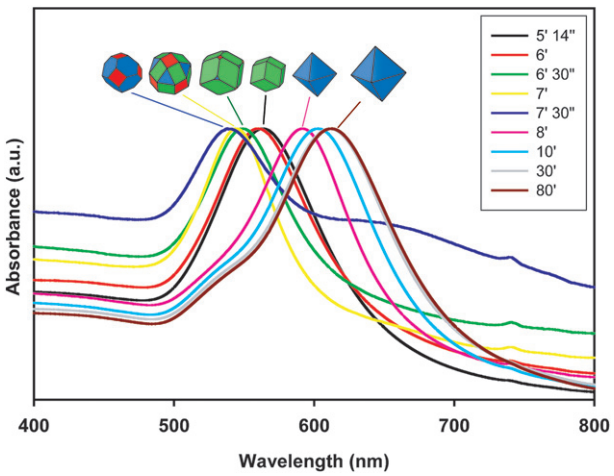

Fig. 4 UV/Vis spectra of the gold nanocrystals for various reaction times, with the relevant schematic structure shown in each inset. The absorption spectra are gradually blue-shifted from the rhombic dodecahedron to the truncated octahedron as a result of truncation and are abruptly red-shifted once the octahedron with sharp edges is produced.

length of ~75 nm is abruptly red-shifted to 590 nm due to the formation of sharp edges after further growth; the octahedral nanocrystals with an edge length of ~90 nm still exhibit a red-shifted absorption peak at 603 nm. The growth of the octahedral nanoparticles becomes saturated after 30 min of reaction time and the edge length and the absorption peak of the particles become ~100 and 610 nm, respectively. The UV/Vis absorption spectra are consistent with the proposed evolution of particle shape with reaction time and provide further evidence for the involvement of etching and growth in the evolution of crystal shape and size.

We have demonstrated the potential applications of gold nanoparticles which have different plasmon resonance wavelengths in cell imaging.[26,27] Fig. 5 shows the dark field light scattering image of macrophage cells (RAW 264.7) treated with three different PEG-coated gold nanoparticles (truncated octahedra (540 nm), rhombic dodecahedra (565 nm), octahedra (603 nm)). Compared to the dark field image of macrophage cells (Fig. 5-a), strong scattering signals were detected from the macrophage cells labeled with PEG-coated gold nanoparticles. Furthermore, the enhanced scattering-based optical contrast in macrophage cells were dependent on the plasmon resonance wavelength of each gold nanoparticles (Fig. 5b,c,d). Our experimental results imply that the gold nanoparticles having different shapes that preferentially scatter light of choose color can be used in multiplex applications in biology and medicine.

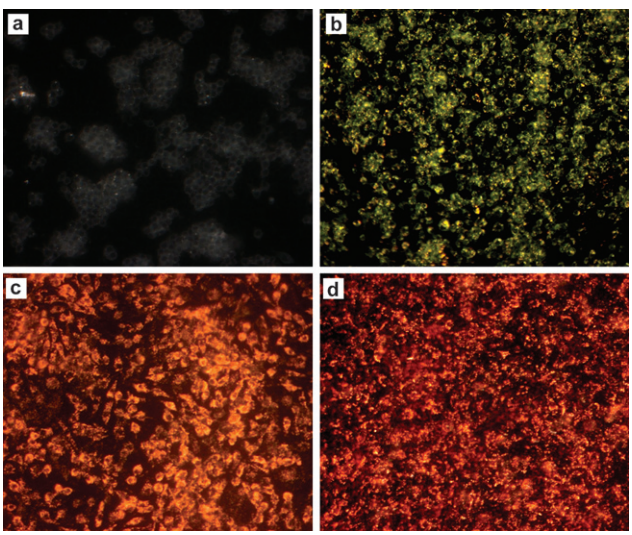

Fig. 5 Dark-field light scattering images of macrophage cells (RAW264.7) treated with three different PEG-coated gold nanoparticles. (a) RAW 264.7, (b) truncated octahedra, (c) rhombic dodecahedra, and (d) octahedra.

Conclusions

In summary, the shapes of gold nanocrystals with O_h symmetry prepared with colloidal chemistry using DMF as a solvent and reducing agent are strongly dependent on the concentration of water in our experimental conditions. At lower concentrations of water (1.4 mL), the rhombic dodecahedral nanocrystals are transformed into octahedral nanocrystals *via* rhombicuboctahedral and truncated octahedral particles because the etching reaction contributes to the elimination of the edges and/or to the hindrance of the addition of atoms onto the edges and the growth reaction proceeds so as to minimize the surface energy. At higher concentrations of water (2 mL), the rhombic dodecahedral nanoparticles are transformed into cubes or truncated cubes *via* rhombicuboctahedra due to the suppression of addition onto the {100} face and the activation of addition onto the {110} and {111} faces as a result of enhanced etching and growth. The cubes or truncated cubes are transformed into truncated octahedra or cuboctahedra, which are the thermodynamically more stable nanoparticles. The elucidation of the transformations of the nanocrystals with O_h symmetries provides a method for the synthesis of shape-controlled nanocrystals and opens the door to a range of interesting studies of the control of the shapes, sizes, and morphologies of metal nanoparticles. Moreover we demonstrated that such shape controlled gold nanoparticles could be used in multiplex applications in biology and medicine.

Acknowledgements

This work was supported by the WCU (World Class University) program through the Korea Science and Engineering Foundation (KOSEF) funded by the Ministry of Education, Science and Technology (MEST) (No. R32-2008-000-10142-0).

References

1 C. Burda, X. Chen, R. Narayanan and M. A. El-Sayed, *Chem. Rev.*, 2005, **105**(4), 1025.
2 R. Jin, Y. Cao, C. A. Mirkin, K. L. Kelly, G. C. Schatz and J. G. Zheng, *Science*, 2001, **294**, 1901.
3 R. Jin, Y. Cao, E. Hao, G. S. Métraux, G. C. Schatz and C. A. Mirkin, *Nature*, 2003, **425**, 487.
4 V. F. Puntes, K. M. Krishnan and A. P. Alivisatos, *Science*, 2001, **291**, 2115.
5 C. Salzemann, I. Lisiecki, A. Brioude, J. Urban and M.-P. Pileni, *J. Phys. Chem. B*, 2004, **108**, 13242.
6 Y. Xia, P. Yang, Y. Sun, Y. Wu, B. Mayers, B. Gates, Y. Yin, F. Kim and H. Yan, *Adv. Mater.*, 2003, **15**, 353.
7 Y. Cao, R. Jin and C. A. Mirkin, *Science*, 2002, **297**, 1536.

8 N. L. Rosi and C. A. Mirkin, *Chem. Rev.*, 2005, **105**, 1547.
9 B. D. Moore, L. Stevenson, A. Watt, S. Flitsch, N. J. Turner, C. Cassidy and D. Graham, *Nat. Biotechnol.*, 2004, **22**, 1133.
10 A. J. Haes and R. P. Van Duyne, *J. Am. Chem. Soc.*, 2002, **124**, 10596.
11 K. Kneipp, Y. Wang, H. Kneipp, L. T. Perelman, I. Itzkan, R. R. Dasari and M. S. Feld, *Phys. Rev. Lett.*, 1997, **78**, 1667.
12 F. Kim, S. Connor, H. Song, T. Kuykendall and P. Yang, *Angew. Chem., Int. Ed.*, 2004, **43**, 3673.
13 D. Seo, J. C. Park and H. J. Song, *J. Am. Chem. Soc.*, 2006, **128**, 14863.
14 C. Li, K. L. Shuford, Q.-H. Park, W. Cai, Y. Li, E. J. Lee and S. O. Cho, *Angew. Chem., Int. Ed.*, 2007, **46**, 3264.
15 A. Sánchez-Iglesias, I. Pastoriza-Santos, J. Pérez-Juste, B. Rodríguez-González, F. J. García de Abajo and L. M. Liz-Marzán, *Adv. Mater.*, 2006, **18**, 2529.
16 N. R. Jana, L. Gearheart and C. J. Murphy, *J. Phys. Chem. B*, 2001, **105**, 4065.
17 T. K. Sau and C. J. Murphy, *J. Am. Chem. Soc.*, 2004, **126**, 8648.
18 E. Carbó-Argibay, B. Rodríguez-González, J. Pacifico, I. Pastoriza-Santos, J. Pérez-Juste and L. M. Liz-Marzán, *Angew. Chem., Int. Ed.*, 2007, **46**, 8983.
19 D. Seo, C. I. Yoo, J. C. Park, S. M. Park and H. J. Song, *Angew. Chem., Int. Ed.*, 2008, **47**, 763.
20 L. D. Mark, *Rep. Prog. Phys.*, 1994, **57**, 603.
21 Z. L. Wang, *J. Phys. Chem. B*, 2000, **104**, 1153.
22 A. V. Gaikwad, P. Verschuren, S. Kinge, G. Rothenberg and E. Eiser, *Phys. Chem. Chem. Phys.*, 2008, **10**, 951.
23 J. Xu, S. Li, J. Weng, X. Wang, Z. Zhou, K. Yang, M. Liu, X. Chen, Q. Cui, M. Cao and Q. Zhang, *Adv. Funct. Mater.*, 2008, **18**, 277.
24 B. J. Wiley, S. H. Im, Z.-Y. Li, J. McLellan, A. Siekkinen and Y. Xia, *J. Phys. Chem. B*, 2006, **110**, 15666.
25 J. P. Kottmann and O. J. F. Martin, *Phys. Rev. B: Condens. Matter Mater. Phys.*, 2001, **64**, 235402.
26 C. J. Murphy, A. M. Gole, J. W. Stone, P. N. Sisco, A. M. Alkilany, E. C. Goldsmith and S. C. Baxter, *Acc. Chem. Res.*, 2008, **41**, 1721.
27 D. A. Schultz, *Curr. Opin. Biotechnol.*, 2003, **14**, 13.